13th International Conference on Flow-induced Vibration
Paris, France
7-10th July 2026

FIV2026 -676695
Prediction of the motion amplitude of vertical flexible cylinders due to wind excitation by vortex shedding using a revised effective correlation length model

Agathe Schmider[1,2] & Pascal Hémon[1]
[1] *LadHyX, CNRS-Ecole Polytechnique, IP Paris, France*
[2] *EPFL, Lausanne, Switzerland (Current address)*

Keywords : *vortex shedding, wind loads, turbulence, chimney*

1. INTRODUCTION

The prediction of the response of flexible vertical cantilevered circular cylinders, such as industrial chimneys, undergoing wind-induced excitation, is still a challenge from an engineering point of view. Current models, such as the two methods from the Eurocode framework (Ruscheweyh and Vickery–Basu simplified models), remain limited in their ability to predict oscillation amplitude. The Ruscheweyh's model, also known as the "effective correlation length model", has the advantage to incorporate physical parameters related to the vortex shedding process. This paper offers improvements to the parameters' values in the model supported by experimental evidence. The objective is to align the set of parameters as closely as possible with the actual physics of vortex shedding, using experimental observations in turbulent flows typical of wind engineering.

2. THE BOUIN EXPERIMENT

We report the measurements performed on a full-scale vertical cylinder subject to natural wind. Preliminary results were presented in (Ellingsen et al. 2022; Schmider & Hémon 2025) and we provide here the oscillation amplitude to be used to adjust the prediction model and compare the results with these observations. Figure 1 shows the experimental setup off the chimney erected at Bouin (France) near the Atlantic seashore, for measurement of the vortex shedding excitation (Manal & Hémon, 2024).

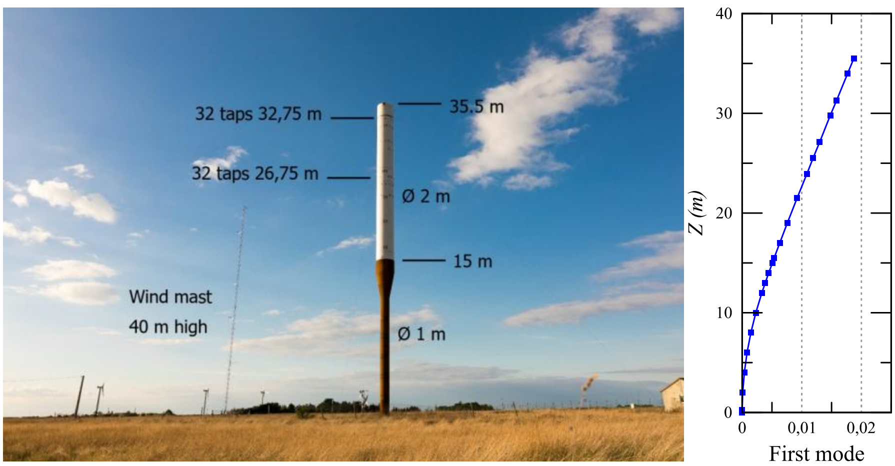

Figure. 1. Photo of the Bouin chimney with its dimensions and computed shape of the first bending mode

Typical Reynolds number is around 1.1 million. The chimney is a 35.5 m high steel tube with an external diameter of 1 m in the lower part, from 0 to 12 m, and 2 m in the upper part above 15 m. From 12 to 15 m the diameter linearly increases from 1 to 2 m. The upper part has an aspect ratio L/D equal to 10. The chimney is clamped at the bottom in a concrete mass properly designed. Structural properties of the chimney are given in Table 1. The Scruton number

$Sc = \frac{4\pi m\eta}{\rho D^2}$ is 1.53. Due to the specific design of the chimney the computed first bending mode shown in Figure 1 has a quasi-linear shape in its upper part.

Four single component accelerometers are mounted to measure the chimney motion (type PCB 3741). They can measure in the frequency range [0-70 Hz] up to ±2 g with an accuracy better than ±0.04 g. Accelerometers #1 and #2 are fixed at a height of 20.4 meters and #3 and #4 at the top, ie 35.5 meters. The record is continuous with a sampling frequency of 16 Hz. In the following, only the top accelerometers are used, providing the amplitude of the motion which is based on the first bending mode.

Parameters	Symbol	Value	Unit
Linear mass	m	322.6	kg/m
Reduced damping	η	0.185	%
First bending frequency	f	0.848	Hz

Table 1. Structural parameters of the chimney

The statistical results are given in Table 2 and plotted in Figure 2 as a function of the reduced frequency $f_r = \frac{f\,D}{\bar{U}}$. The peak amplitude of the chimney's response is $\frac{Y_{max}}{D} = g\,\frac{Y_{rms}}{D}$ in which g is the peak factor. Four sequences approach a "perfect" lock-in, with an amplitude that reaches 36 % of the diameter. The corresponding Strouhal number is 0.225. The other sequences present much lower amplitudes, lower than 10 % of the diameter. In these cases, the chimney response is certainly due to the turbulent excitation with a small contribution of the vortex shedding.

The measured amplitudes are compared to the estimations obtained from the two methods of Eurocode, using a simplified Ruscheweyh's model (Eurocode 1) or Vickery-Basu model (Eurocode 2), and are shown in Figure 2(left). The Vickery-Basu model overestimates the field observations (0.53 against 0.36), while Ruscheweyh's model underestimates them (0.21 against 0.36).

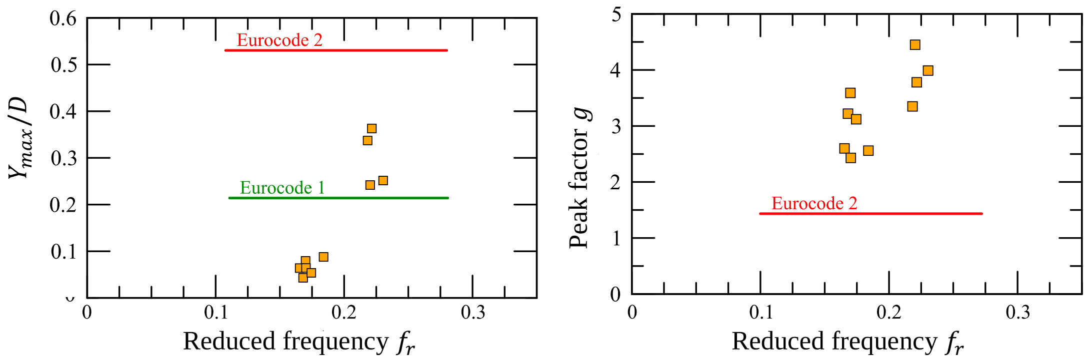

Figure 2. Measured maximum top amplitude (left) and peak factor (right) versus reduced frequency.

Date	Time	f_r	Y_{max}/D	Y_{RMS}/D	g
19-07-21	16h50	0.2203	0.2418	0.0543	4.45
	17h00	0.2216	0.3630	0.0961	3.78
	17h10	0.2183	0.3372	0.1006	3.35
	17h20	0.2304	0.2516	0.0630	3.99
20-07-21	14H00	0.1681	0.0431	0.01337	3.22
	14h10	0.1700	0.0788	0.02210	3.59
	14h20	0.1654	0.0638	0.02463	2.60
	14h30	0.1840	0.0874	0.03430	2.56
	12h40	0.1703	0.0641	0.02638	2.43
	12h50	0.1745	0.0537	0.01724	3.12

Table 2. Measured top amplitude

Moreover, the measured peak factors are shown in Figure 2(right) and compared to the Eurocode prediction from method 2, which greatly underestimates the observations. Simultaneously, the amplitude is already overestimated, which reinforces the unadequate representation of the physical behavior by this method for the present case. These disagreements prove that some improvements should be made on the prediction model. In this paper we propose further revised parameter values of the correlation length model with the idea of respecting as much as possible the physics of the vortex shedding phenomenon that we observed.

3. THE EFFECTIVE CORRELATION LENGTH MODEL

We recall here the original method of prediction introduced by Ruscheweyh (1985, 1994) which was later simplified to become the method 1 in the Eurocode (2005). The principle of the model is based on the harmonic excitation of the cylinder by a lateral force $C_y(z)$ which depends on the altitude z. This force is applied to the bending mode $\phi(z)$ of the cylinder. The assumption is made that the frequencies of the vortex shedding f_{vs} and of the bending mode f are the same because this is the situation which generates the maximum amplitude of motion.

We define the reduced frequency $f_r = \frac{f\,D}{\bar{U}}$ and the Strouhal number $St = \frac{f_{vs}\,D}{\bar{U}}$. When resonance occurs the frequency of vortex shedding is equal (or close) to the frequency of the chimney, *ie* $f_{vs} = f$ which defines the critical velocity $\bar{U} = U_c$ and then $f_r = St$.

At resonance, the RMS amplitude of the response of the chimney can be written

$$\frac{Y_{rms}}{D} = \frac{\rho\, U_c{}^2}{8\pi\,\delta\, m_e\, f^2}\,\frac{\int_0^H C_y(z)\,\phi(z)\,dz}{\int_0^H \phi(z)^2\,dz} \tag{1}$$

in which $\delta = 2\pi\eta$ is the log decrement of the structure having a reduced damping η referred to critical damping; m_e is the effective mass calculated with the linear mass distribution $m(z)$ of the chimney applied to the bending mode:

$$m_e = \frac{\int_0^H m(z)\,\phi(z)^2\,dz}{\int_0^H \phi(z)^2\,dz} \tag{2}$$

The main idea of the method is to assume an ideal periodic force distributed between the heights a and b with a RMS value C_{lat} as shown in Figure 3. The length $b - a = L_c$ is the effective correlation length which gave its name to that method. The load term can be rewritten as

$$\int_0^H C_y(z)\,\phi(z)\,dz = C_{lat}\int_a^b \phi(z)\,dz \tag{3}$$

so that the expression is simplified in

$$\frac{Y_{rms}}{D} = \frac{C_{lat}}{Sc\;St^2}\;K\;K_w \tag{4}$$

where the shape factor, depending on the shape of the bending mode, is

$$K = \frac{\int_0^H \phi(z)\,dz}{4\pi\int_0^H \phi(z)^2\,dz} \tag{5}$$

while the correlation length factor is

$$K_w = \frac{\int_a^b \phi(z)\,dz}{\int_0^H \phi(z)\,dz} \tag{6}$$

which depends on the heights a and b. Note that in the Eurocode the end effect is neglected, leading to $s = 0$ and $b = H$, while a value of $s = 1.5\,D$ is suggested by Ruscheweyh (1985).

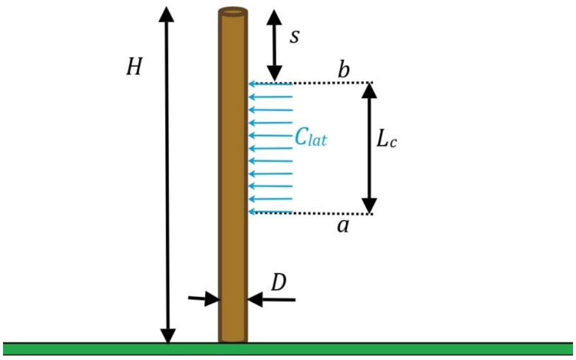

Figure 3. Idealized load distribution as in (Ruscheweyh 1985)

In the case of a parabolic deflection, which is $\phi(z) = \left(\frac{z}{H}\right)^2$, these two factors are

$$K_w = \frac{3L_c}{H}\left[1 - 2\frac{s}{H} + \left(\frac{s}{H}\right)^2 - \frac{L_c}{H}\left(1 - \frac{s}{H}\right) + \frac{1}{3}\left(\frac{L_c}{H}\right)^2\right] \text{ and } K = 0.133 \tag{7}$$

In the case of linear deflection $\phi(z) = \frac{z}{H}$ then

$$K_w = 2\frac{L_c}{H}\left[1 - \frac{s}{H} - \frac{1}{2}\frac{L_c}{H}\right] \text{ and } K = 0.119 \tag{8}$$

The correlation length L_c is a function of the maximum amplitude of oscillation, using the function proposed by Ruscheweyh (1994)

$$\frac{L_c}{D} = 2\, e^{1+1.4\frac{Y_{0\,max}}{D}} \tag{9}$$

which is limited to $\frac{Y_{0\,max}}{D} < 0.6$. For higher amplitudes of oscillation, the correlation length is limited to $\frac{L_c}{D} = 12$. Note that the Eurocode proposes a simplified calculation of the correlation length in function of the oscillation amplitude which is close to Ruschweyh's original formula.

The peak factor g is the ratio between the maximum and the RMS values. It is equal to $\sqrt{2}$ for a perfect harmonic signal and increases to about 4 for a Gaussian signal. It has been proposed, (Ruscheweyh & Sedlacek, 1988), following the analysis by Vickery & Basu (1983) to estimate the peak factor with a function that depends on the ratio of the structural damping to aerodynamic damping η/η_a:

$$g = \sqrt{2}\left[1 + 1.2\, arctan\left(0.75\, \left(\frac{\eta}{\eta_a}\right)^4\right)\right] \tag{10}$$

With this expression, when the structural damping and consequently the Scruton number are small, the peak factor remains close to $\sqrt{2}$. This expression is used by method 2 of Eurocode.

4. REVISED VALUES OF SOME COEFFICIENTS OF THE PREDICTION MODEL

4.1. The lateral force coefficient

The lateral force coefficient C_{lat} is a key parameter of the prediction model: for Reynolds numbers between 0.5 to 5 millions, the Eurocode suggest that $C_{lat} = 0.2$ which comes from the upper envelope of a series of collected data as shown in (Ruscheweyh & Sedlacek, 1988).

Here we measure the force thanks to two series of 32 wall pressure taps at the altitude of 26.75 and 32.75 m (Hémon et al. 2025). The latter is close to the top, at $1.4\,D$ of the chimney's end (see also Figure 1). The pressure signals are processed using the bi-orthogonal decomposition technique to isolate the term which is responsible for the lateral force and to filter, at least partially, the turbulent component.

Two cases are reported here, the first with the chimney at rest thanks to stay cables and another case with small oscillations at $f_r = 0.17$. Results are given in Table 3 where an estimated uncertainty of 10 % applies to C_{lat}. The values of C_{lat} are well in accordance with previous works (Ruscheweyh, 1985) but they are lower than 0.2 which is prescribed in Eurocode.

The peak factor of the force observed during the 10 minutes sequence is also reported. Values are larger than the theoretical value of $\sqrt{2}$, particularly near the top, showing the influence of a stochastic behavior, even on an a priori harmonic phenomenon.

Altitude (m)	f_r	Y_{max}/D	C_{lat}	g of C_{lat}
26.75	0	0	0.153	3.20
26.75	0.17	0.0164	0.165	3.20
32.75	0	0	0.155	4.39
32.75	0.17	0.0164	0.143	4.33

Table 3. Measured lateral force coefficients on the Bouin chimney

4.2. The peak factor

At resonance, the peak factor measured on the Bouin's chimney is much larger than the one theoretically estimated because this estimation assumes a steady harmonic motion. Indeed, in real conditions, it almost impossible to observe such a stationary response to wind during a period of 10 minutes. In 1964 Alan Davenport (Davenport 1964) proposed a formula of the peak factor based on the assumption that the observed signal is long enough and Gaussian. This formula reads

$$g = \sqrt{2\, ln(\nu\, T)} + \frac{0.577}{\sqrt{2\, ln(\nu\, T)}} \tag{11}$$

where T is the observation time and ν is a quantity that can be "interpreted physically as the frequency at which most of the energy in the spectrum is concentrated" (Davenport 1964). In our case, the frequency is the one of the bending mode ν=0.848 Hz and the observation time is T=600 s. Numerical application of the Davenport's formula gives $g = 3.69$. Figure 4 compares the experimental peak factors with the results from the application of Davenport's formula and gives a better agreement than the suggestion from Eurocode method 2.

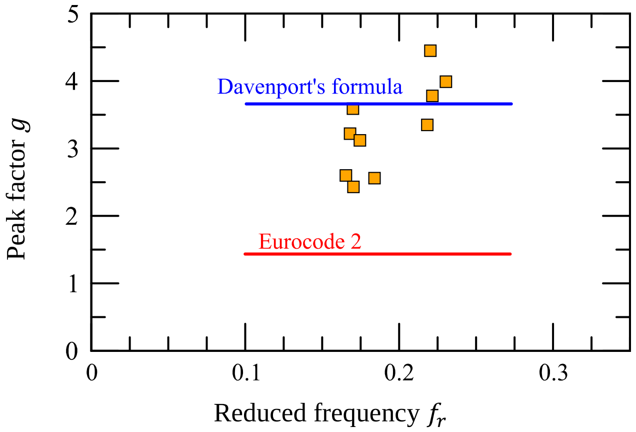

Figure 4. Measured and computed peak factors versus reduced velocity.

4.3. New measurements of the effective correlation length

In this section, we present new wind tunnel measurements of the correlation length using modern measurement and processing techniques in the context of a wind-excited chimney. The upstream turbulence characteristic is varied with a focus on the large length scales.

The objective is to present new measured data in the wake of a rigid cantilevered cylinder in function of the upstream turbulence characteristics. This kind of measurement is unachievable in field tests, which justifies the use of wind tunnel testing, despite the shortcomings such as the reduced scale and the low Reynolds number.

The cylinder models are made of brass tubes of diameter D = 5 mm and 1 mm thick. The hole is filled by a 3 mm stainless steel rod which stops 10 mm (2 D) below the top, for increased rigidity while keeping a tube-like extremity. The whole is strongly clamped below the wind tunnel floor. The cylinder height is 88 mm that corresponds to the aspect ratio of the Bouin chimney (17.6).

In the wake of this model, two hot-wire probes are mounted separately using elbow supports (see Figure 5). Each probe is attached to a manual linear translation stage, one positioned above and one below the test section, so that their vertical position can be easily adjusted. The positions of the probes are read on a steel rule, with a rough accuracy of 0.5 mm. The hot-wires are located 15 mm (3D) downstream the cylinder axis and with a lateral offset of 2.5 mm (0.5 D) from the cylinder axis.

The setup shown in figure 5 is designed to measure, for a fixed altitude Z, the correlation coefficient and the coherence between the two hot-wire probes, in function of their distance ΔZ.We note $u_1(t)$ and $u_2(t)$ the two measured velocities, $\bar{U}_1$ and $\bar{U}_2$ their time-averaged values, σ_1 and σ_2 their standard deviation, and n the number of samples. The correlation coefficient is defined as

$$R_{12}(\Delta Z) = \frac{\sum_t (u_1(t)-\bar{U}_1).(u_2(t)-\bar{U}_2)}{n\ \sigma_1\ \sigma_2} \tag{12}$$

This scalar quantity varies between -1 and +1. It quantifies how the two signals are synchronized. The integral correlation length scale L_R is defined by integration of this coefficient:

$$L_R = \int_{-\infty}^{+\infty} R_{12}(\Delta z)\, d\,(\Delta z) = 2\int_0^{+\infty} R_{12}(\Delta z)\, d\,(\Delta z) \tag{13}$$

The physical meaning of L_R is the length along the vertical axis for which the correlation is 1.

In the wake of the cylinder, this quantity reflects how the unsteady fluctuations, such as the vortex shedding, are simultaneous along the vertical axis. However, the correlation coefficient accounts for all fluctuations of the velocity, including those from turbulence and from vortex shedding.

Therefore, another quantity, physically representative of the vortex shedding phenomenon, is needed. Noting $S_{11}(f)$ and $S_{22}(f)$ the power spectral densities of the two velocities $u_1(t)$, $u_2(t)$, and $S_{12}(f)$ their cross power spectral density, we define the coherence as

$$Coh_{12}(f) = \frac{|S_{12}(f)|^2}{S_{11}(f)\ S_{22}(f)}\,. \tag{14}$$

This function in the Fourier domain is between 0 and 1. We extract this value at the frequency of vortex shedding f_{vs} and use this scalar quantity in the same manner as the correlation coefficient. The integral coherence length scale L_{coh} is then defined by

$$L_{coh} = 2\int_0^{\infty} Coh_{12}(f_{vs})\, d\,(\Delta z) \tag{15}$$

The integral coherence length scale reflects the vertical span of the vortex shedding, filtered from the turbulent fluctuations.

In the rest of the paper, the integral length scales L_R and L_{coh}, and the spacing ΔZ will be reduced by the diameter D. Global uncertainty resulting from the measurements and the integration process is estimated to be of the order of 0.1 D.

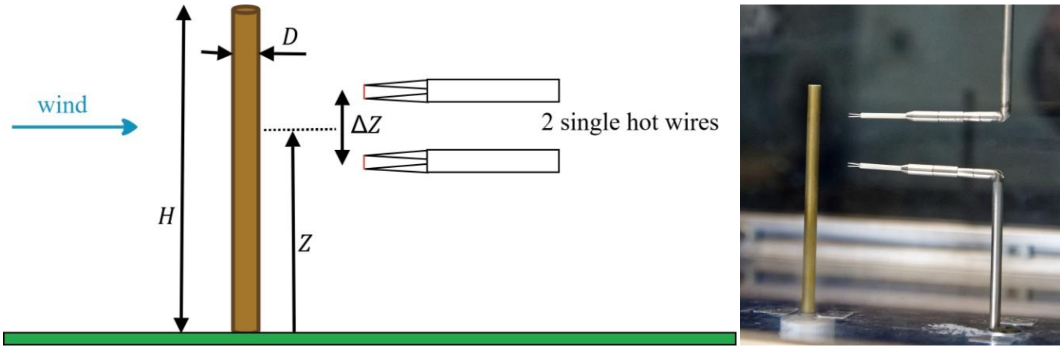

Figure 5. Sketch and picture of the measurements in the wake of the cylinder.

The reference velocity U_{ref} is measured with a double Pitot tube mounted through the ceiling of the test section and connected to a pressure sensor (Furness Control, type FCO 332) regularly calibrated. This velocity is corrected from the air temperature and the atmospheric pressure according to the ideal gas law. Temperature is continuously measured by a K-type thermocouple located along the Pitot tube, while the atmospheric pressure is manually read twice a day on a mercury barometer. Final accuracy is better than 1%.

The other measurement devices are two hot wire probes controlled by two constant temperature anemometers (Dantec, type Mini CTA 54T30). We used two kinds of probes, a set of two single wires (Dantec, type P11), or a double wire probe (Dantec, type P61). The single wire probes are devoted to the longitudinal velocity component $u(t)$ while the double probe can deliver both longitudinal and lateral component $v(t)$. The cable length between the probes and the anemometers is 5 m.

Hot-wire anemometers are calibrated in situ in the empty test section with the reference speed U_{ref} from the pitot tube. The relationship between the output voltage from the anemometer and the air flow speed in m/s is fitted to a third degree polynomial with a correlation coefficient superior to 0.9999. The flow speed measured during the experiments is corrected according to the temperature difference between the current experiment and the calibrations tests.

Sensors are connected to a Müller-BBM acquisition and processing system (PAK system). The hardware consists of a series of acquisition cards by National Instruments. The analog entry range of ±10 V has a resolution of 24 bits. Each test lasts T = 90 s with a sampling frequency f_e = 10240 Hz. The resulting band pass is 4000Hz, considering the anti-aliasing filter. In the Fourier domain the frequency resolution is Δf = 0.3125 Hz with blocs of 3.2 s.

To identify the flow conditions, a two-component hot-wire probe is mounted at mid-height in the empty wind tunnel. The turbulence characteristics in the wind tunnel are varied by changing the turbulence generator, using a grid, the atmospheric device or a combination of both. The atmospheric device is a patented system (2024) which generates a turbulent flow with length scales exceeding the cylinder diameter, which a turbulence grid cannot achieve. Finally, four kinds of flow are obtained:

a. Smooth flow with very low turbulence level without generator
b. Turbulent flow with short length scales generated by the grid
c. Turbulent flow with large length scales generated by the atmospheric device
d. Turbulent flow with intermediate length scales with both the grid and the atmospheric device

The length scales of turbulence are defined here as in the wind engineering domain. They are measured by comparing the measured velocity Power Spectral Density function (PSD) with the model of Von Karman (Diederich & Drischler 1957 ; Von Karman 1948) and by adapting the length scales L_u and L_v to match the experimental curve with the model (Vita et al. 2018). The turbulence intensities and longitudinal and lateral length scales are reported in Table 4.

Device	I_u (%)	I_v (%)	L_u (m)	L_v (m)
None	0.59	0.44	-	-
Grid	8.3	8.1	0.019	0.0055
Atmospheric	10.8	12.7	0.039	0.016
Grid+Atmospheric	8.9	10.3	0.027	0.015

Table 4. Turbulence characteristics measured with the two-component hot-wire probe.

Figure 6 reports the measured integral coherence and correlation length scales as a function of the mean height and the type of incoming turbulence. The type of flow turbulence greatly influences the integral lengths and most particularly the integral coherence length.

Under atmospheric flow, the integral coherence length is less than half of that in smooth flow but stays at a significant level over a wider height range: the integral coherence length L_{coh} exceeds 3.75 D for Z/H between 0.35 and 0.7.

Integral coherence and correlation lengths decrease closer to the top end of the cylinder under all turbulence conditions. The gradient of this decrease is steeper in smooth flow than in atmospheric turbulence.

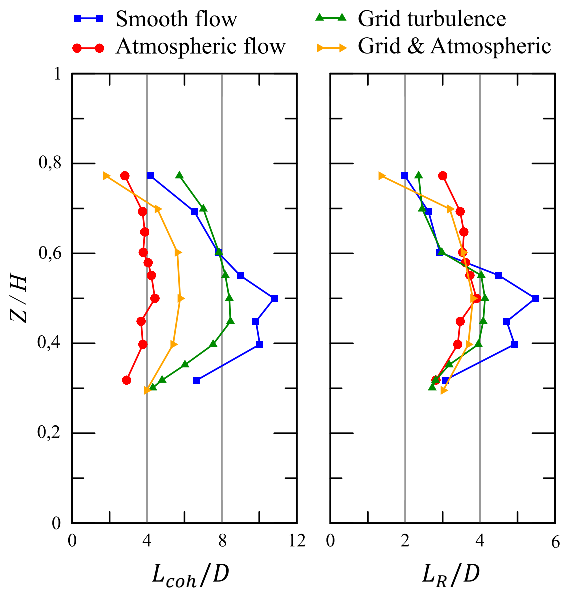

Figure 6. Integral length scales versus altitude for aspect ratio 17.6.

5. COMPARISON OF PREDICTION WITH EXPERIMENTS

As a conclusion, we now apply the revised parameters to the Bouin chimney, *i.e.* the end effect, the coherence length, the force coefficient and the peak factor as presented in the previous section.

Table 5 presents the main parameters for the different version of the model. Ultimately, the coherence length L_c/D computed by the different versions is comparable. The end effect is responsible for the large variation on the correlation length factor K_w, with a revised value which is almost half that of the Eurocode.

Model	s/D	L_c/D initial	L_c/D final	K	K_w
Eurocode 1	0	6	7.86	0.119	0.827
Ruscheweyh	1.5	6	7.80	0.119	0.612
Revised model	4	4	7.35	0.119	0.470

Table 5. Parameters of the prediction models for the Bouin chimney

Case	f_r	Y_{max}/D	g
Experiments	0.225	0.363	3.78
Eurocode 1	0.18	0.213	1.41
Ruscheweyh model	0.20	0.258	1.41
Revised model	0.225	0.388	3.69

Table 6. Comparison of maximum amplitude for the Bouin chimney

The comparison of the predictions results with the experiments is presented in the Figure 7 and numerically in the Table 6. The proposed revised model improves significantly the prediction of the maximum amplitude at resonance which was the main goal in terms of engineering studies.

In this favourable result, it is essential to note the importance of the peak factor in the context of the turbulent wind excitation: while the other revised parameters contribute to decrease the prediction of the oscillation amplitude, it is the peak factor that allows to find the value close to the experimental results. The main advantage is that all the parameters of the model are found as close as possible to the physics of the phenomenon of wind-induced vortex excitation, as it be seen in Table 6 where the measured peak factor is very close to the predicted value by the Davenport formula.

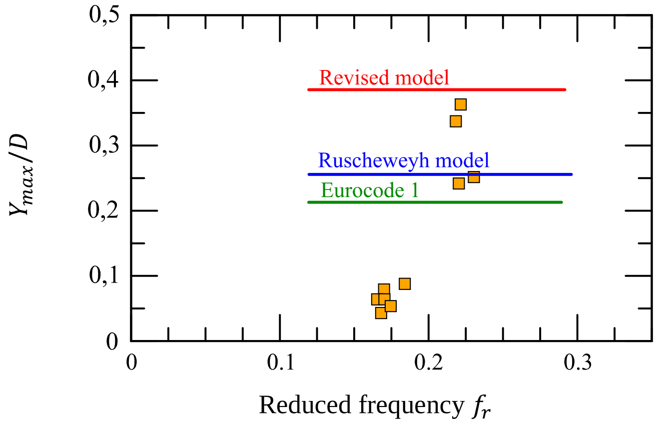

Figure 7. Measured and computed maximum top amplitude versus reduced velocity.

Acknowledgements

The Bouin experiment was included in a partnership co-funded by Beirens (Poujoulat Group), Centre Scientifique et Technique du Bâtiment (CSTB), Centre National d'Etudes Spatiales (CNES) and LadHyX, CNRS-Ecole Polytechnique.

REFERENCES

Davenport, A.G., 1964. Note on the distribution of the largest value of a random function with application to gust loading. In: Proceedings of the Institution of Civil Engineers. pp. 187–196.

Diederich, F.W., Drischler, J.A., 1957. Effect of spanwise variations in gust intensity on the lift due to atmospheric turbulence. NACA TN 3920.

Ellingsen Ø., Flamand O., Amandolese X., Coiffet F., Hémon P., 2022. Field tests on a full-scale steel chimney subjected to vortex-induced vibrations. *Structural Engineering International*, 32, 55-61.

Eurocode, 2005. Actions on structures – Part 1-4: General actions – Wind actions. European committee for standardization, Brussels.

Hémon, P., Kurniawati, I., Lupi, F., Seidel, M., Höffer, R., 2025. An estimation of the unsteady lateral force on two full scale large vertical cylinders submitted to natural wind. 9th European African Conference on Wind Engineering,p. 345-348, June 16-19, Trondheim, Norway.

Manal, Y., Hémon, P., 2024. Unsteady loads on circular cylinder in cross-flow: An observation in natural wind and comparison with wind tunnel experiments. *Journal of Fluids and Structures* 124, 104019.

Patent, 2024: Dispositif générateur de turbulence atmosphérique basse altitude et soufflerie associée. Numéro de dépôt 2407134. CNRS-Ecole Polytechnique.

Ruscheweyh, H., Sedlacek, G., 1988. Crosswind vibrations of steel stacks. Critical comparison between some recently proposed codes. J. *of Wind Engineering & Industrial Aerodynamics* 30, 173–183.

Ruscheweyh, H., 1985. The vortex excited amplitude. RWTH Aachen report.

Ruscheweyh, H., 1994. Vortex excited vibrations. In "Wind-Excited Vibrations of Structures", edited by H. Sockel, Springer-Verlag, Wien, 51–84.

Schmider, A., Hémon, P., 2025. Vortex-induced vibrations measured on a full scale chimney. 9th European African Conference on Wind Engineering, p. 341-344, June 16-19, Trondheim, Norway.

Vickery, B.J., Basu, R.I., 1983. Across-wind vibrations of structures of circular cross-section. Part I. Development of a mathematical model for two-dimensional conditions. *J. of Wind Engineering & Industrial Aerodynamics* 12(1), 49–73.

Vita, G., Hemida, H., Andrianne, T., Baniotopoulos, C.C., 2018. Generating atmospheric turbulence using passive grids in an expansion test section of a wind tunnel. *J. of Wind Engineering & Industrial Aerodynamics* 178, 91-104.

Von Karman, T., 1948. Progress in the statistical theory of turbulence. *Proc. Nat. Acad. Sci*., 34 (11), 530-539.